Nonlinear Compensation in Optical Communications Systems With Normal Dispersion Fibers Using the Nonlinear Fourier Transform

Ivan T. Lima Jr., *Senior Member, IEEE, Senior Member, OSA*, Thiago D. S. DeMenezes, Vladimir S. Grigoryan, Maurice O'Sullivan, and Curtis R. Menyuk, *Fellow, IEEE, Fellow, OSA*

***Abstract*—We investigate the computational cost of the nonlinear Fourier transform (NFT) based on the Zakharov–Shabat scattering problem as a nonlinear compensation technique for quadrature-phase-shift keyed (QPSK) signals with raised cosine frequency characteristic in optical fiber transmission systems with normal dispersion fibers. We show that the primary sources of computational errors that arise from the use of the NFT is the finite eigenvalue resolution of the left and the right reflection spectra. We show that this effect and, consequently, the computational cost of the NFT as a nonlinear mitigation technique in the normal dispersion regime increases exponentially or faster with both the channel power and the number of symbols per data frame even using the most efficient NFT algorithms that are currently known. We find that the computational cost of this approach becomes unacceptably large at data frame lengths and powers that are too small for this approach to be competitive with standard transmission methods. We explain the physical reasons for these limits.**

***Index Terms*—Discrete transforms, fiber nonlinear optics, optical fiber communication, signal processing algorithms.**

I. Introduction

NONLINEARITY in optical fibers limits the achievable signal-to-noise ratio and, consequently, the transmission capacity of optical fiber communications systems [1]. The principal source of nonlinearity in optical fibers is the Kerr nonlinearity, and it has been known since the 1980s that to lowest order in the nonlinearity strength and chromatic dispersion, light propagation can be modeled by the nonlinear Schrödinger equation (NLSE) [2], [3]. The NLSE is one of a very special class of nonlinear equations that can be solved using a nonlinear analogue of the Fourier transform [4], [5] that was first found by Zakharov and Shabat [6]. In general, this transformation will produce both a discrete (solitons) and continuous (reflection) spectrum. Due to the nonlinearity, the evolution of initial data in the time domain can be quite complex, but all this complexity disappears in the transform domain, and the evolution becomes linear and quite simple. It is this observation that is at the heart of efforts in the 1980s and 1990s to use solitons in communications systems, since the evolution of solitons is simple in systems that obey the NLSE.

With the advent of coherent communications and advanced signal processing techniques in optical fiber communications systems, this basic idea has undergone a renaissance. Yousefi and Kschischang [7]–[9] have proposed to combine high-order soliton solutions with advanced signal processing techniques to achieve high spectral efficiency.

Several research groups have investigated the use of the continuous spectrum of the Zakharov-Shabat scattering problem (ZSSP) [9]–[13]. This approach has some attractive features. First, the continuous spectrum reduces to the usual Fourier transform at low intensities, so that it is possible to carry over standard modulation formats in a straightforward way. Second, a continuous spectrum can be generated in both the normal and the anomalous dispersion regimes, while a discrete spectrum (solitons) can only be generated in the anomalous dispersion regime.

Experimental studies have demonstrated the use of the NFT for nonlinear mitigation uisng the discrete spectrum [14]–[16] and both the discrete and the continuous spectrum [17]. These studies use the Darboux transform as the INFT algorithm, which was combined in [17] with the INFT algorithm in [10] to reconstruct the waveform from the nonlinear spectrum using both the continuous and the discrete part of the spectrum. However, the symbol rates, the spectral efficiency, and the total signal bandwidth in these studies is still well below those of current optical fiber transmission systems.

While the idea of using the continuous spectrum is attractive, work to date has pointed to several issues that must be addressed if this idea is going to have practical value. First, the computational complexity of carrying out the analogue of the Fourier transform and its inverse is high. The nonlinear Fourier transform (NFT) and its inverse (INFT) are given by the solution to the ZSSP. In the forward direction, the most widely

Manuscript received November 2, 2016; revised February 24, 2017 and July 21, 2017; accepted October 10, 2017. Date of publication October 25, 2017; date of current version November 16, 2017. *(Corresponding author: Ivan T. Lima Jr.)*

I. T. Lima Jr. and T. D. S. DeMenezes are with the Department of Electrical and Computer Engineering, North Dakota State University, Fargo, ND 58108-6050 USA (e-mail: Ivan.Lima@ndsu.edu: Thiago.DeMenezes@ndsu.edu).

V. S. Grigoryan is with the Ciena Corporation, Hanover, MD 21076 USA (e-mail: vgrigory@ciena.com).

M. O'Sullivan is with the Ciena Corporation, Ottawa, ON K2H 8E9 Canada (e-mail: mosulliv@ciena.com).

C. R. Menyuk is with the Department of Computer Science and Electrical Engineering, University of Maryland Baltimore County, Baltimore, MD 21250 USA (e-mail: menyuk@umbc.edu).

Color versions of one or more of the figures in this paper are available online at http://ieeexplore.ieee.org.

Digital Object Identifier 10.1109/JLT.2017.2766622

used computational methods have a computational complexity that is proportional to N^2, where N is the number of points in the waveform that is being processed [18], [19]. In the backward direction (INFT), the most commonly used methods have a computational complexity that is either proportional to N^2 in differential layer peeling methods [20] or $N^2 \log N$ in the integral layer peeling method [21]. The complexity of these methods scales too rapidly with N to be acceptable in practice. Wahls *et al.* [22], [23] recently proposed NFT and INFT algorithms that scale proportional to $N \log^2 N$. However, it was shown in [23] that the fast NFT that they developed breaks down when the magnitude of the left reflection spectrum is significantly lower than what can be achieved with the integral layer peeling method. Since higher launch powers and longer frame durations lead to magnitudes of the left reflection spectrum very close to 1, achieving high power levels with fast NFT algorithms is still a challenge.

Work to date points to the existence of additional problems with algorithms that are based on the ZSSP. These algorithms rely fundamentally on the assumption that the signal is zero at the edges of the time domain that is being considered. For this reason, the data must be carved into data frames that reside inside larger signal frames or total time frames that are sufficiently large to accommodate any spread in the data that is due to chromatic dispersion. In this respect, these systems resemble orthogonal frequency domain multiplexed (OFDM) systems [24]. In studies to date of the NFT and INFT in both the normal [25], [26] and the anomalous [10] dispersion regimes, the data frame only occupies a small fraction of the total time frame. In the normal dispersion regime, the fraction occupied was a little over 1% [25]; in the anomalous dispersion regime, the fraction occupied was a little over 10% [10]. The data frame occupies such a small percentage of the total frame because of the relatively small size of the data frame compared with the required guard time that is needed to prevent inter-frame cross-talk due to chromatic dispersion. The duration of the guard time is proportional to the second-order dispersion parameter, the signal bandwidth, and the propagation distance.

There are reasons to believe that there may be a limit to the size of the data frames that can be used with the NFT for a finite number of points used to discretize the left reflection spectrum. In the normal dispersion regime, the waveform encoding the symbols act as barriers in the forward ZSSP. As the reflection coefficient approaches 1 with the increase in the frame duration, the waveform containing the symbols in the center of the data frame become increasingly difficult to resolve. In the anomalous dispersion regime, for a fixed power, standard estimates indicate that the number of solitons should grow with the data length [5]. Wahls *et al.* [22] also developed an NFT algorithm for periodic signals, but further work is needed to assess the effectiveness of the NFT for periodic signals.

Just as there may be limits on the size of the data frames, there may be limits on the signal power within those frames. In the anomalous dispersion regime, increased power is expected to lead to soliton generation [5]. In the normal dispersion regime, increase of the channel power or the data frame lead to an increase in the number of points used to discretize the reflection spectrum.

There are two approaches for the encoding and decoding of data that can be carried out using the NFT. The NFT can be used to encode data directly on the eigenvalues of the ZSSP at the transmitter using an INFT algorithm, which is decoded with the NFT at the receiver [9], [10]. The other approach uses the NFT as a digital-back-propagation algorithm at the receiver to compensate for the nonlinearity and the dispersion along the direction of propagation [25]. In this work, we investigate the latter application of the NFT for data decoding at the receiver while using standard QPSK encoding at the transmitter.

We analyze the scaling of the back end processing time as a function of the signal power and the size of the data frame. To do so, we used the same quaternary-phase-shift-keyed (QPSK) format that Le *et al.* [10] studied, although we focus here on the normal dispersion regime. We find that the use of the NFT and the INFT in the signal processing results in a computational cost that grows exponentially with the channel power and the data frame duration. For realistic fiber parameters, the onset of this exponential growth occurs at a combination of signal powers and data frame lengths that are too low for this scheme to be competitive as an alternative to standard quasilinear transmission. When the channel power is set to 3 dBm in a QPSK modulation format at 56 Gbaud with 512 symbols per data frame, the number of points required to discretize each of the reflection spectra exceeds 2^{103}. We stress that this exponential increase in the back end processing time is not due to the computational complexity of the algorithms. Rather, it is a limitation of the method, which is due to the rapid increase in the resolution of the reflection spectra that is required to decode the waveform. The increase in the required spectral resolution of the reflection spectra arises because it contains all the necessary information to decode the signal at any distance.

In [13], a nonlinear OFDM signal with launch power per data frame equal to 0 dBm was simulated with 15 channels with 4 GHz of bandwidth per channel in an optical fiber transmission system with second-order dispersion parameter $\beta_2 = 21.7$ ps^2/km with 16,384 points to discretize the reflection spectrum. The reflection spectrum at that power corresponds to the reflection spectrum at -6.37 dBm of average launch power per data frame in the optical fiber transmission system with $\beta_2 = 5$ ps^2/km that we consider here. In [12], a fast NFT and a fast INFT algorithm was used to decode and digitally back-propagate a waveform in a fiber transmission system with $\beta_2 = 20.4$ ps^2/km. Despite using 65,536 points to discretize the reflection spectrum of QPSK data frame with 128 symbols at 56 GBd, the performance peaked at 3 dBm of average launch power per data frame, which corresponds to -6.07 dBm of channel power due to the required guard time. The reflection spectrum required for this fiber at 3 dBm of average launch power corresponds to -3.23 dBm of average launch power per data frame in the fiber that we consider in this study. The results of those studies are consistent with our finding that the number of points required to discretize the reflection spectrum and, consequently, the computational cost of the NFT to mitigate the

nonlinear Kerr effect increases rapidly just when the nonlinear distortion becomes significant.

The remainder of this paper is organized as follows: In Section II, we review the ZSSP and we describe the computational algorithms that we used to solve the NFT and INFT and the motivation for our choices. In Section III, we present numerical results relating the computational cost of the NFT and the INFT as a function of the launch power and the frame duration. In Section IV, we describe the underlying reasons for the exponential increase of the computational cost of the NFT and the INFT with both the launch power and the frame duration. We find that the limits on the data frame length and signal power are surprisingly low compared to quasilinear systems. Section V contains the conclusion.

II. Numerical Methods

The time and the space dependence of the slowly varying envelope of the optical signal propagating in optical fibers is modeled by the nonlinear Schrödinger (NLS) equation [27],

$$i\frac{\partial A(t,z)}{\partial z}+i\frac{\alpha(z)}{2}-\frac{\beta_2}{2}\frac{\partial^2 A(t,z)}{\partial t^2}+\gamma\left|A(t,z)\right|^2A(t,z)=0, \tag{1}$$

where $A(t,z)$ is the slowly varying envelope of the optical signal, z is the space coordinate along the direction of propagation, γ is the nonlinear parameter, β_2 is the second-order dispersion parameter, and $\alpha(z)$ is the attenuation coefficient or gain. The most efficient techniques to solve the NLS equation in optical fiber communications systems is the split-step Fourier method. In the particular case in which the losses can be either neglected or mitigated through the use of distributed amplification ($\alpha \cong 0$), the normalized slowly varying envelope of the optical signal $q(t,z)$ satisfy the ZSSP, which is defined in terms of the [6]

$$\begin{aligned}\frac{du(t,\zeta)}{dt}&=i\zeta u(t,\zeta)+q(t,z)v(t,\zeta),\\ \frac{dv(t,\zeta)}{dt}&=-i\zeta v(t,\zeta)+q^*(t,z)u(t,\zeta),\end{aligned} \tag{2}$$

where $u(t,\zeta)$ and $v(t,\zeta)$ are the eigenfunctions of the ZSSP associated to the eigenvalue ζ. The eigenfunctions also depend implicitly on z. To apply the ZSSP in (2) to optical fibers with the slowly varying envelope of the optical signal $A(t,z)$, we use the expression

$$q(t,z)=\sqrt{\frac{\gamma}{|\beta_2|}}A(t,z). \tag{3}$$

The term $(\gamma/|\beta_2|)^{1/2}$ in (3) is the normalization coefficient of the ZSSP, so that (2) can be applied to lossless optical fibers with arbitrary nonlinear parameter γ and second-order dispersion β_2.

The QPSK frame of symbols is located near the center of the computation time window $[0, T_w]$ with boundary conditions $A(0,z)=A(T_w,z)=0$ for $z\in[0,L]$, where L is the propagation distance. The left and the right reflection spectra at the receiver are given by

$$r_L(\zeta,L)=\left.\frac{v(0,\zeta)}{u(0,\zeta)}\right|_{v(T_w,\zeta)=0}\quad r_R(\zeta,L)=\left.\frac{u(T_w,\zeta)}{v(T_w,\zeta)}\right|_{u(0,\zeta)=0}. \tag{4}$$

The advantage of using the reflection spectra to represent the waveform, compared to the Fourier spectrum, is that the magnitude of the reflection spectra at each eigenvalue ζ does not change with z if the medium does not have losses. Moreover, the phase of the reflection spectra evolves linearly, so that the reflection spectra calculated at the receiver can be propagated forward or backward to any point along z using a single propagation step that compensates for the combined effects of nonlinearity and dispersion along the transmission. The reflection spectra at the transmitter ($z=0$) can be computed from the calculated reflection spectra at the receiver ($z=L$) using the

$$\begin{aligned}r_L(\zeta,0)&=r_L(\zeta,L)\exp\left(+i2\zeta^2\beta_2L\right),\\ r_R(\zeta,0)&=r_R(\zeta,L)\exp\left(-i2\zeta^2\beta_2L\right).\end{aligned} \tag{5}$$

It is the resolution in ζ that is required to accurately determine the original data that in turn determines the value of T_w. In practical cases, the value of T_w is much larger than that of a single data frame.

A. Nonlinear Fourier Transform

In this work, we use the piece-wise constant approximation (PCA) to calculate the NFT [19] or, equivalently, to solve the direct scattering problem. Most studies so far have only made use of the left reflection spectrum. However, there is no computational cost required to calculate the right reflection spectrum together with the left reflection spectrum using the PCA method. Moreover, there is also little additional computational cost in using both the left reflection spectrum, to construct the first half of the time-domain waveform of the optical signal in our computation of the INFT, and the right reflection spectrum, to construct the second half of the time-domain waveform, in our computation of the same INFT. The most efficient methods to compute the INFT are based on iterative procedures, whose computational error accumulates as the number of iterations increases. The computational error in the symbols near the right end of the frame dominate the overall computational error of INFT procedures that use only the left reflection spectrum. Therefore, the error in our computation of the INFT is significantly reduced when the waveform is reconstructed from both ends of the data frame in time domain.

To calculate both the left and the right reflection spectra using the PCA, we follow the procedure described in [20]. For every eigenvalue ζ, we calculate the evolution of the eigenfunctions during each time-step Δ_t,

$$\begin{bmatrix}u\left(t_{m+1},\zeta\right)\\ v\left(t_{m+1},\zeta\right)\end{bmatrix}=\mathbf{T}_{m+1}(\zeta)\begin{bmatrix}u\left(t_m,\zeta\right)\\ v\left(t_m,\zeta\right)\end{bmatrix}, \tag{6}$$

where $t_m = m\Delta_t$,

$$\mathbf{T}_m(\zeta) = \begin{bmatrix} \cosh(k\Delta_t) \\ +i\zeta \sinh(k\Delta_t) & q(t_m, z)\sinh(k\Delta_t) \\ q^*(t_m, z)\sinh(k\Delta_t) & \cosh(k\Delta_t) \\ & -i\zeta \sinh(k\Delta_t) \end{bmatrix}, \quad (7)$$

and $k^2 = |q|^2 - \zeta^2$. We then calculate the transmission matrix

$$\mathbf{T}(\zeta) = \prod_{m=1}^{N_{\text{pt}}-1} \mathbf{T}_m(\zeta), \quad (8)$$

where N_{pt} is the number of points used to discretize the waveform in the time domain. For a given eigenvalue ζ, the left and the right reflection spectra in (4) can be calculated,

$$r_L(\zeta) = \frac{-T_{2,1}(\zeta)}{T_{2,2}(\zeta)}, \; r_R(\zeta) = \frac{T_{1,2}(\zeta)}{T_{2,2}(\zeta)}. \quad (9)$$

The eigenvalue spectral range is defined from $-\pi/(2\Delta_t)$ to $\pi/(2\Delta_t)$. If the eigenvalue range is discretized with N_{pt} points, the eigenvalue resolution Δ_ζ is given by $\Delta_\zeta = \pi/(N_{\text{pt}}\Delta_t)$. The eigenvalues of the ZSSP that we compute are evenly spaced because practical INFT methods make use of the Fourier transform and/or the inverse Fourier transform of the reflection spectra. The computational complexity of the PCA is proportional to $N_{\text{samp}} \times N_{\text{pt}}$, where the constant of proportionality is the number of operations used to evaluate the 2×2 complex matrix in (5) and to carry out a 2×2 complex matrix multiplication.

B. Inverse Nonlinear Fourier Transform

The first computational method to solve the INFT consisted of integral equations developed by Gelfand, Levitan, and Marchenko [28]. However, due to the high computational complexity required to directly solve the GLM integral equations (N^3), more efficient iterative methods have been developed [20], [21], [29]–[33].

The differential layer peeling (DLP) method is one of the most efficient INFT methods [31]. The DLP method iteratively solve the GLM integral equations with computational complexity proportional to $N_{\text{samp}} \times N_{\text{pt}}$, where N_{samp} is the number of samples used to discretize the waveform in time domain and N_{pt} is the total number of points used to discretize the left reflection spectrum [20], [30], [31]. The DLP method that is applied to fiber grating design requires that the reflection coefficient from within a discrete space step be small enough so that the reflection coefficient of that layer can be lumped at the end of the discrete space step [30]. Otherwise, the computational error in the result produced by the DLP algorithm, which increases exponentially along the direction of the profile extraction, would be unacceptably high. For that reason, strong gratings, in which the reflection coefficient is close to 1 over a large spectral band, require a large number of steps along the grating for the DLP to produce accurate results. In the optical fiber communications problem that we are considering, a QPSK modulation format with -3 dBm of channel power and 56 GBd per data frame requires time steps that are significantly smaller than the symbol period.

Rosenthal and Horowitz [21] developed an inverse scattering algorithm—denoted the integral layer peeling (ILP) method—that consists of solving the GLM integral equations for each layer using an iterative procedure that includes the recursive calculation of the local reflection spectrum, starting with the left reflection spectrum in (9). Because the errors in the ILP accumulate with the number of iterations, as it is the case in the other iterative methods for calculating the INFT, we decided to implement and use the symmetric ILP (SILP) method. In the SILP method, the left portion of the waveform is computed from the left edge of the waveform up to the center of the time window, using the left reflection spectrum. Then, the right portion of the waveform is computed from the right edge of the waveform until the center of the time window, using the right reflection spectrum.

The SILP method uses the Born approximation to define the local reflection spectra at the time $t_{m+1} = t_m + \Delta_t$,

$$r_{L,m+1}(\zeta) = \frac{r_{L,m}(\zeta) - \bar{r}_{L,m}(\zeta)}{1 - r_{L,m}\bar{r}^*_{L,m}(\zeta)} \exp(-i2\zeta\Delta_t),$$
$$r_{R,m+1}(\zeta) = \frac{r_{R,m}(\zeta) - \bar{r}_{R,m}(\zeta)}{1 - r_{R,m}\bar{r}^*_{R,m}(\zeta)} \exp(-i2\zeta\Delta_t), \quad (10)$$

where

$$\bar{r}_{L,m}(\zeta) = \int_{-\infty}^{2\Delta_t} h_{L,m}(\tau)\exp(i\zeta\tau)\,d\tau,$$
$$\bar{r}_{R,m}(\zeta) = \int_{(\pi/\Delta_\zeta)-2\Delta_t}^{\infty} h_{R,m}(\tau)\exp(-i\zeta\tau)\,d\tau, \quad (11)$$

and

$$h_{L,m}(\zeta) = \int_{-\infty}^{\infty} r_{L,m}(\tau)\exp(-i\zeta\tau)\,d\tau,$$
$$h_{R,m}(\zeta) = \frac{1}{2\pi}\int_{-\infty}^{\infty} r_{R,m}(\tau)\exp(i\zeta\tau)\,d\tau, \quad (12)$$

are the Fourier transform of the left-local reflection spectrum and the inverse Fourier transform of the right-local reflection spectrum, respectively. The local reflection spectra at $m = 0$ are the reflection spectra calculated with the PCA algorithm in (9). The recovered waveform at the discrete time $t_m = m\Delta_t$ is given by:

$$A(t_m, z) = \sqrt{\frac{\beta_2}{\gamma}} \times \begin{cases} -h_{L,m}(t_{m+1}), & m \le N_{\text{samp}}/2 \\ h_{R,m}(t_{N_{\text{samp}}-m+1}), & m > N_{\text{samp}}/2 \end{cases}. \quad (13)$$

To minimize the discretization error of the NFT-INFT algorithms, we shift $A(t_m, z)$ by $\Delta_t/2$ in the frequency domain at the end of the INFT. This procedures improves the accuracy of the NFT-INFT algorithms, especially at low sampling rates.

Since only N_{samp} values of the time-domain waveform are generated by the SILP metthod, whose reflection spectra have a much larger number of discrete values, N_{pt}, it is necessary to shift the time in the reflection spectra prior to the execution of the iterative procedure in (10)–(13):

$$r_{L,0}(\zeta) = r_L(\zeta)\exp\left[-i\zeta\Delta_t(N_{\text{pt}} - N_{\text{samp}})/2\right],$$
$$r_{R,0}(\zeta) = r_R(\zeta)\exp\left[-i\zeta\Delta_t(N_{\text{pt}} - N_{\text{samp}})/2\right]. \quad (14)$$

The SILP method is capable of extracting the profile of gratings whose reflection coefficient is very close to 1 across a wide spectral band. The computational error of the SILP method does not accumulate as fast as with the DLP method, enabling the SILP method to reconstruct gratings with reflectivity as large as $1-10^{-10}$ [21]. Even though the computational complexity of the SILP is $N_{\text{samp}} \times N_{\text{pt}} \cdot \log N_{\text{pt}}$, as needed to solve (10)–(13), this method converges significantly faster than the DLP method in [31] when applied to strong gratings, which correspond to optical signals with channel powers above −3 dBm.

Belai *et al.*, developed an alternative method to solve the GLM integral equations based on the iterative inversion of Toeplitz matrices obtained from the GLM integral equations that was denoted Toeplitz inner-bordering (TIB) [33] that has numerical complexity equal to N_{pt}^2 when the iterative matrix inversion procedure is optimized. This method was shown to perform comparably to the ILP method when the magnitude of the left reflection spectrum is below 0.99994 [23], which corresponds to data frames in the quasi-linear regime. When these results are extended to optical fiber communications systems operating in the normal dispersion regime, the maximum magnitude of the reflection spectra, these results correspond to channel powers in the quasi-linear regime of operation.

Due to the demonstrated high robustness of the SILP method in the nonlinear regime, in which the magnitude of the reflection spectra is very close to 1, such as $1-10^{-9}$, over a wide range of the eigenvalue ζ, we chose the SILP method as the INFT algorithm in this study. A careful comparison of the performance of different INFT algorithms is beyond the scope of this study, especially because we observed that the primary reason for the rapid increase in the computational cost of the use of the NFT-INFT algorithms with the increase of the channel power is due to the rapid increase of the required resolution of the left and/or right reflection spectra.

C. Modulation Format

We simulate each data frame with a sequence of symbols using the QPSK modulation format with raised cosine frequency characteristics as in [34]. We simulate the raised cosine frequency characteristic using a matched receiver filter, in which the transmitted signal has a root raised cosine frequency characteristic, and the receiver filter has a transfer function $H(f)$ that is a root raised cosine frequency function given by

$$H(f)=\begin{cases}1, & |f| \le \dfrac{1-\epsilon}{2T_s} \\ \cos\left[\dfrac{\pi T_s}{2\epsilon}\left(|f|-\dfrac{1-\epsilon}{2T_s}\right)\right], & \dfrac{1-\epsilon}{2T_s} < |f| \le \dfrac{1+\epsilon}{2T_s} \\ 0, & |f| > \dfrac{1+\epsilon}{2T_s}\end{cases}, \tag{15}$$

where T_s is the symbol period per data frame and ϵ is the roll-off factor.

The algorithms that we chose to carry out the NFT-INFT computation (PCA and the SILP) are applied to the waveform before the receiver filter. These algorithms could in principle be implemented experimentally by applying a digital filter whose transfer function is close to the inverse of the receiver filter in (15) after the signal is demultiplexed and optically filtered at the receiver. Then, after the left and the right reflection spectra are digitally propagated backward to the transmitter and the waveform is extracted from the reflection spectra using the SILP method, the signal is passed through a filter whose transfer function is shown in (15).

TABLE I
THE RATIO (IN dB) OF THE CHANNEL POWER AND THE AVERAGE LAUNCH POWER PER DATA FRAME ($P_{\text{ch}}/P_{\text{df}}$), THE EFFECTIVE SYMBOL RATE (f_s), AND THE SPECTRAL EFFICIENCY (SE) FOR A QPSK MODULATION FORMAT AT 56 GBd PER DATA FRAME AS A FUNCTION OF THE NUMBER OF SYMBOLS PER DATA FRAME FOR 1,000 KM OF PROPAGATION DISTANCE

Symbols / Frame	$P_{\text{ch}}/P_{\text{df}}$ (dB)	f_s (GHz)	SE (bits/s/Hz)
32	−6.7	11.9	0.43
64	−4.5	19.7	0.70
128	−2.8	29.1	1.04
256	−1.7	38.3	1.37
512	−0.9	45.5	1.62

D. Channel Power and Effective Symbol Rate

In addition to the requirement that the transmission systems do not have losses for the eigenvalues to remain constant during the fiber transmission, the nonlinear parameter γ, along with the second-order dispersion β_2, must remain constant. Therefore, each data frame with a fixed number of symbols has to be separated by a guard time that is large enough to ensure that the dispersed frames do not produce inter-data frame cross-talk along the transmission due to the nonlinearity and, more importantly, they do not produce inter-data frame interference at the receiver. Therefore, the requirement of the guard time leads to a reduction in the channel power, given the average launch power per data frame, and a reduction in the effective symbol rate, given the symbol rate in the data frame. The guard time t_g required to accommodate the chromatic dispersion along the fiber transmission line is given by

$$t_g = t_{g,R} \times 2\pi|\beta_2| f_{s,\text{df}} \cdot L, \tag{16}$$

where $f_{s,\text{df}}$ is the symbol rate in the data frame, $t_{g,R}$ is the relative guard time, and L is the length of the fiber transmission system. In the results shown here, we used $t_{g,R} = 1.2$, which provides a 20% margin for the guard time, as in [10]. Given the guard time in (16), the channel power P_{ch} is given by

$$P_{\text{ch}} = \frac{N_{\text{sym}}}{N_{\text{sym}} + t_g \cdot f_{s,\text{df}}} P_{\text{df}}, \tag{17}$$

where P_{df} is the average launch power per data frame and N_{sym} is the number of symbols per data frame. The effective symbol rate f_s is given by

$$f_s = \frac{N_{\text{sym}}}{N_{\text{sym}} + t_g \cdot f_{s,\text{df}}} f_{s,\text{df}}. \tag{18}$$

In Table I, we show the difference in dB between the average launch power and the channel power in dB, the ratio between the symbol rate per data frame and the effective symbol rate, and

the spectral efficiency for 56 GBd QPSK systems with 32, 64, 128, 256, and 512 symbols per data for 1,000 km of propagation distance. Therefore, it is desirable to have the number of symbols per data frame as large as possible in order to minimize the performance degradation due to the guard time.

E. System Model and Performance Metric

We use the Q-factor calculated from the error-vector magnitude (EVM) [35], [36] due to computational errors from the nonlinear compensation using the NFT as the performance metric. Each simulation consists of the following steps:

1) We generate the QPSK waveform from a randomly-chosen data frame and propagate it through all the spans of a lossless and noise-free optical fiber transmission system modeled by (1) using the adaptive split-step Fourier method presented in [37], which is third-order accurate. This split-step Fourier method automatically adjusts the step size to keep the local error constant.
2) We apply the PCA method to the received waveform.
3) We propagate the reflection spectra in the backward direction to the transmitter using a single step, as shown in (5).
4) We apply the SILP method to reconstruct the waveform at the transmitter.
5) We apply a time-shift in the frequency domain on half the time step to cancel the time shift between the NFT and the INFT;
6) We filter the reconstructed waveform using the transfer function in (15).
7) We calculate the EVM in the data frame.
8) We repeat the steps 1–6 30 times, and we calculate the Q-factor from the average EVM. In a QPSK system, the Q-factor is given by

$$Q = \left(\frac{1}{N} \sum_{n=1}^{N} \mathrm{EVM}_n \right)^{-1}. \tag{19}$$

We calculate the Q-factor using 30 randomly-chosen data frames to reduce the variance in the calculation.

III. Results and Discussions

We use computer simulations to assess the effectiveness of signal processing techniques based on the ZSSP applied to optical fiber communications systems in the normal dispersion regime. The optical fiber that we consider has second-order dispersion $\beta_2 = 5$ ps^2/km and nonlinear parameter $\gamma = 1.27$ (W$\cdot$ km)$^{-1}$. These parameters are close to those of commercially available single-mode fiber and to those used in [25]. The total propagation distance that we consider is equal to 1,000 km. We use the QPSK modulation format with the raised cosine spectral characteristic described in Section II-C with a roll-off factor $\epsilon = 1/7$. We use the PCA method to solve the NFT and the SILP method that we presented in Section II-B to solve the INFT. When executing the PCA and the SILP methods, we minimize the computational cost of those methods by only calculating the NFT and the INFT for the smallest number of samples in the time domain that are sufficient to accommodate the frame duration and the guard time. In Fig. 1, we show the schematic representation of the steps 1 through 4 shown in Section II-E applied to a QPSK system with 128 symbols at 56 GBd per data frame with a channel power equal to −2.8 dBm. The number of points used to discretize each of the reflection spectra, $N_{\mathrm{pt}} = 2^{17}$, is the smallest number of points—in powers of two—that produces a $Q > 15$ dB due to discretization errors in the PCA-ILP algorithms.

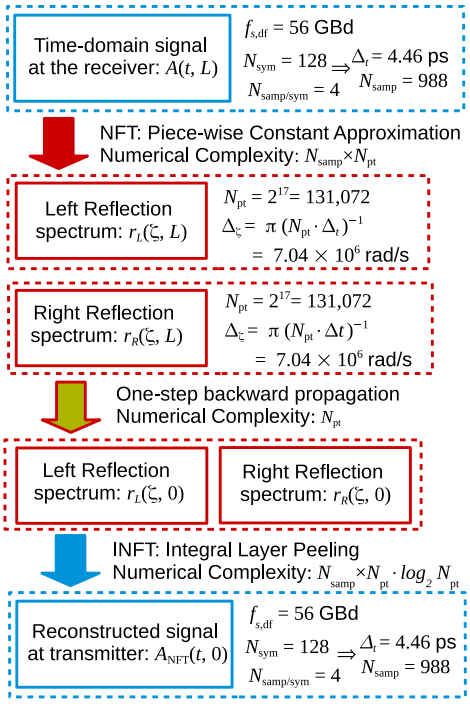

Fig. 1. Schematic diagram of the nonlinear mitigation technique based on the NFT. We use here the PCA to compute the NFT and the SILP to compute the INFT. The numbers here are applicable to a QPSK waveform with 128 symbols at 56 GBd per data frame and −2.8 dBm of channel power (0 dBm of average launch power per data frame) with 4 samples per symbol and relative guard time $t_{g,R} = 1.2$, resulting in a total of $(128 + 119) \times 4 = 988$ samples. The reflection spectra are discretized with 2^{17} points.

A. Reflection Spectra

In this sub-section, we investigate the dependence of the reflection spectra resolution on the channel power. Unlike the equivalent representation of the waveform in the Fourier domain, the reflection spectra in (4) and (9), which account for the combined effects of nonlinearity and dispersion along the fiber transmission, are also dependent on the channel power.

In Fig. 2, we show the squared magnitude of the left reflection spectrum of a QPSK waveform at 56 GBd per data frame with 128 symbols, 1,000 km of lossless propagation distance, and relative guard time $t_{g,R} = 1.2$, which corresponds to an effective symbol rate of 29 GBd. The left reflection spectrum is shown at −8.8 dBm of channel power (−6 dBm of average launch power per data frame) with 2 samples per symbol and −2.8 dBm of channel power (0 dBm of average launch power per data frame) with 4 samples per symbol. The number of samples per symbol used in each case was the minimum number of samples that

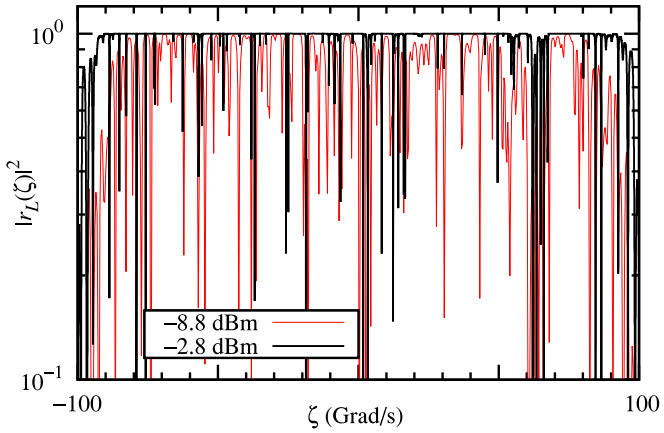

Fig. 2. Squared magnitude of the left reflection spectrum as a function of the eigenvalue ζ for channel power equal to −8.8 dBm (with 2^{10} points) with 2 samples per symbol and −2.8 dBm (with 2^{17} points) with 4 samples per symbol with 128 QPSK symbols per symbol at 56 GBd per data frame with 1,000 km of lossless propagation distance and relative guard time $t_{g,R} = 1.2$, which corresponds to and effective symbol rate of 29 GBd. The channel power is −2.8 dB lower than the average launch power per data frame.

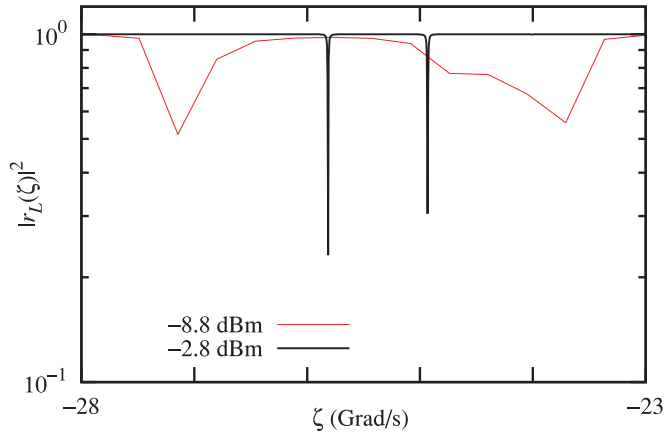

Fig. 3. The same results shown in Fig. 2 for the eigenvalue ζ from −28 to −23 Grad/s.

enabled $Q > 15$ dB due to numerical errors in the NFT-INFT algorithms. Therefore, the larger sample rate required by the NFT could be achieved using upsampling. We observed that the system with −8.8 dBm of channel power has a left reflection spectrum whose magnitudes are clustered toward 1, but vary broadly between 0 and 1. By contrast, in the system with −2.8 dBm of channel power, the magnitude of the non-zero left reflection spectrum is close to 1 at almost all values of ζ. However, the left reflection spectrum is punctuated by a set of sharp spikes that must be resolved in order to accurately calculate the INFT. The largest value of the left reflection spectrum magnitude with −2.8 dBm of channel power is equal to $1 - 1.9 \times 10^{-9}$, while the largest value of the left reflection spectrum magnitude with −8.8 dBm of channel power is equal to 0.9993. The maximum possible value that the reflection spectra magnitudes in (9) in a system with positive second-order dispersion can take is equal to 1, as in the case of fiber Bragg gratings, and it should approach 1 as the channel power or the number of symbols per data frame increase. Therefore, optical fiber communications systems with normal dispersion fibers and distributed gain that compensates for the fiber loss have reflection spectra that are very close to 1 at channel powers as low as −2.8 dBm with as little as 128 symbols per data frame. If the channel power in this system is increased to as little as −1.2 dBm of channel power (1.7 dB of average launch power per data frame), the magnitude of the left reflection spectrum in at least one of the eigenvalues ζ becomes so close to 1 that it exceeds the accuracy of the floating point numerical representation with double precision, which leads to numerical errors in any INFT algorithm that makes use of the reflection spectra, regardless of the spectral resolution that is used.

In Fig. 3, which was generated using a sub-set of the data shown in Fig. 2, we observed that the QPSK waveform with −2.8 dBm of channel power (0 dBm of average launch power per data frame) requires a much higher eigenvalue resolution of the reflection spectra than the same waveform with −8.8 dBm of channel power (−6 dBm of average launch power per data frame). With −8.8 dBm of channel power and 2^{10} points in each of the reflection spectra, we found that $Q = 20.0$ dB. With −2.8 dBm of channel power and 2^{17} points in the reflection spectra, we found that $Q = 16.6$ dB.

To quantify the rapid increase of the required eigenvalue resolution of the reflection spectra with the channel power, we also calculated the maximum value of the magnitude of the derivative of the left reflection spectrum with respect to the eigenvalue ζ for the results shown in Fig. 2. For −8.8 dBm of channel power, the maximum value of the derivative of the left reflection spectrum with respect to the eigenvalue ζ was equal to 5.80×10^{-9} (rad/s), while for −2.8 dBm of channel power the corresponding number was equal to 3.73×10^{-7} (rad/s). Therefore, a factor of four increase in the channel power produces an increase of two orders of magnitude in the derivative of the left reflection spectrum with respect to the eigenvalue ζ. These results indicate that there is a trade-off between the channel power and the eigenvalue resolution of the NFT, which is one of the main factors that determines the computational cost of the algorithm.

B. NFT and Channel Power

In the previous sub-section, we indicated that the eigenvalue resolution required to apply the NFT to a frame with 128 QPSK symbols at −2.8 dBm of channel power was more than two orders of magnitude higher than the eigenvalue resolution required to apply the NFT to the same QPSK frame with −8.8 dBm of channel power. To investigate the dependence of the computational error of the NFT-INFT algorithms that we used on the channel power, the number of points used to discretize each of the reflection spectra, and the number of QPSK symbols per data frame, we carried out a channel power sweep for eight different number of points used to discretize each of the reflection spectra: 2^{10}, 2^{11}, 2^{12}, 2^{13}, 2^{14}, 2^{15}, 2^{16}, and 2^{17} points, and five different number of symbols per data frame: 32, 64, 128, 256, and 512 symbols. For every channel power, we determined the number of points required in powers of two to discretize each of the reflection spectra that results in $Q > 15$ dB from the

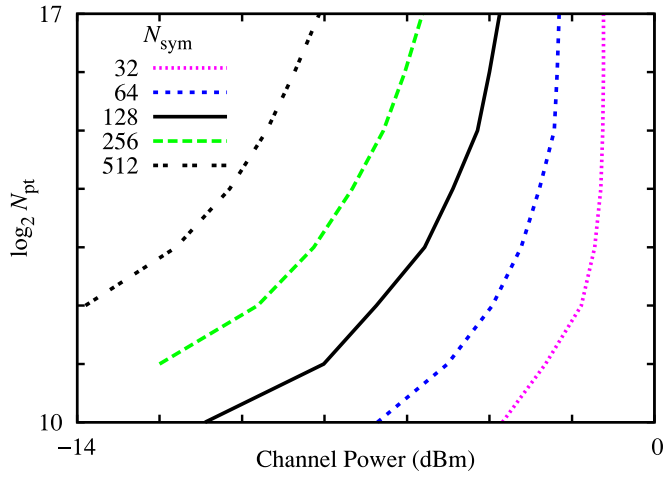

Fig. 4. The logarithm (base 2) of the number of points used to discretize each of the reflection spectra as a function the channel power and $Q > 15$ dB due to the numerical error of the NFT-INFT algorithms. The symbol rate per data frame is equal to 56 GBd and the relative guard time $t_{g,R} = 1.2$. The results are parametrized by the number of symbols per data frame. The Q-factor is calculated from the EVM using 30 randomly-chosen data frames. The difference in dB between the channel power and the average launch power per data frame is given in Table I.

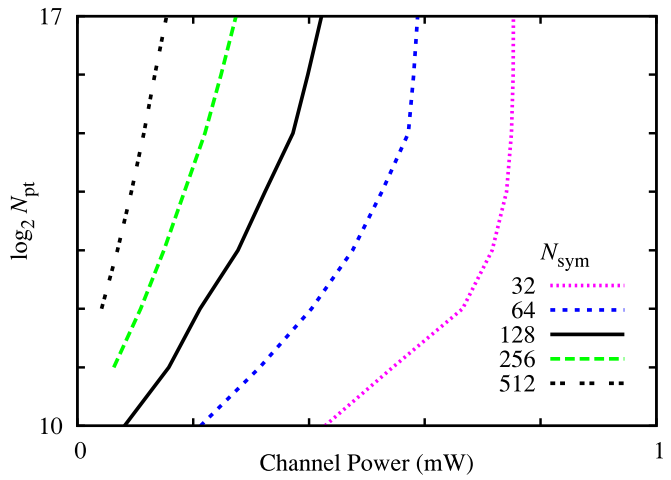

Fig. 5. Same results shown in Fig. 4 presented with the channel power given in mW.

average EVM due to discretization errors in 30 randomly-chosen data frames with the NFT-INFT algorithms. Since the number of samples per symbol in these cases was equal to 4 and the range of eigenvalues ζ is fixed, the increase in the number of points used to represent the reflection spectra increases only the resolution of the reflection spectra. The results of this study are shown in Fig. 4 with the relative guard time $t_{g,R} = 1.2$. At 56 GBd per data frame, the effective symbol rates of: 11.9 GBd for 32 symbols per data frame, 19.7 GBd for 64 symbols per data frame, 29.1 GBd for 128 symbols per data frame, 38.3 GBd for 256 symbols per dta frame, and 45.5 GBd for 512 symbols per data frame. In Fig. 5 we show the same results in Fig. 4 presented with the channel power in linear scale (in mW). We observed that the number of points required to discretize each of the reflection spectra increases exponentially or faster with the channel

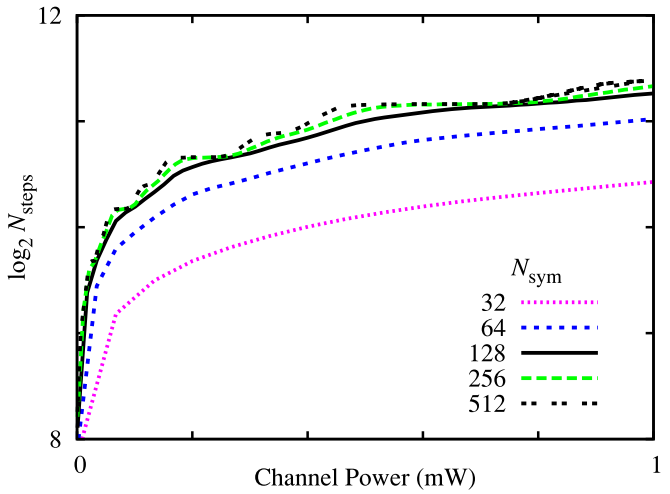

Fig. 6. The logarithm (base 2) of the number of steps in the adaptive split-step Fourier method used for data frames with 32, 64, 128, 256, and 512 symbols. The symbol rate per data frame is equal to 56 GBd and the relative guard time $t_{g,R} = 1.2$. The results are parametrized by the number of symbols per data frame. The number of steps shown is calculated from averaging 30 randomly-chosen data frames. The difference in dB between the channel power and the average launch power per data frame is given in Table I.

power. For the QPSK system with 512 symbols to operate at $Q > 15$ dB at 3 dBm, we extrapolate from the results in Fig. 5 that the reflection spectra have to be discretized with at least 2^{103} points, which is not computationally feasible. Therefore, even if the numerical complexity of the NFT-INFT algorithms could be made as low as that of the Fourier transform ($N \log N$), the computational cost of using the existing NFT-INFT algorithms to encode/decode data would not be practical even when the system is operating a the quasi-linear regime.

To put the rapid increase of the computational cost of the NFT-INFT algorithms with the channel power into perspective, we show in Fig. 6 how the number of steps of the adaptive split-step Fourier method that we use [37] increase with the channel power for the system with 1,000 km with the same 32, 64, 128, 256, and 512 QPSK symbols that were transmitted in Fig. 5. The time and the frequency domain were discretized with 2^{10} points for 32, 64, and 128 symbols, with 2^{11} for 256, and with 2^{12} points for 512 symbols. We observed a much smaller increase of the computational cost with the channel power in the split-step Fourier method when compared to that of the NFT-INFT algorithms.

For the case that we considered here with 128 QPSK symbols at -2.9 dBm of channel power, the NFT method requires a reflection spectra resolution that is sufficiently large to extract the nonlinear evolution of the signal that goes out to to 3×10^5 km of propagation distance, before the signal disperses sufficiently for the nonlinearity to no longer matter. By contrast, the split-step Fourier method only needs to numerically solve the nonlinear evolution of the signal over the system propagation distance, 10^3 km in the case that we consider here. We hypothesize that the reason for the rapid increase of the NFT method with the channel power when compared to the split-step Fourier method is because the reflection spectrum has to contain all the information that is needed to extract the waveform at any

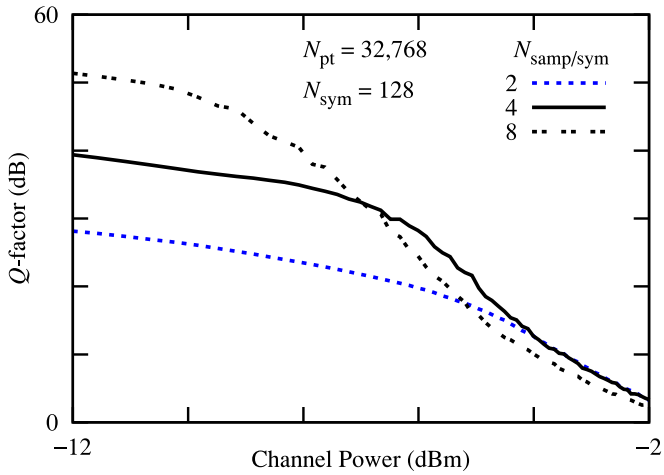

Fig. 7. Q-factor of the received waveform as a function of the channel power for a QPSK waveform with 128 symbols and 56 GBd per data frame with relative guard time $t_{g,R} = 1.2$. The reflection spectra are discretized with 2^{15} points with 2, 4, and 8 samples per symbol. The Q-factor is calculated from the EVM using 30 randomly-chosen data frames. The channel power is −2.8 dB lower than the average launch power per data frame.

distance from 0 km to the distance at which its evolution becomes quasilinear, after which the evolution is fully described by its Fourier modes. While this hypothesis is consistent with our results, as we will discuss in more detail in Section IV-A, a rigorous mathematical analysis has yet to be carried out.

C. NFT and Time Discretization

In Fig. 7, we show the Q-factor due to numerical error in the NFT-INFT algorithms for a QPSK waveform with 56 GBd of symbol rate per data frame and relative guard time $t_{g,R} = 1.2$ as a function of the channel power for 2, 4, and 8 samples per symbol with the reflection spectra discretized with 2^{15} points. At a channel power below −10 dBm, the use of a larger number of samples per symbol produces more accurate results, as shown in Fig. 7. In the linear regime of operation, the residual numerical error reduces by 12 dB for every doubling of the number of samples per symbol. This residual error is the result of the Born approximation, whose accuracy increases with the decrease of Δ_t.

As the average launch power per data frame increases for a fixed number of samples per symbol, the computational error in the calculation of the INFT also increases. This increase in the computational error with the channel power is due to the Born (zero-order) approximation [21], which is used in the SILP method. The computational error due to the Born approximation increases with the channel power, and accumulates with each iteration of the SILP method. We found that the Q-factor decreased slowly with the increase of channel power until reaching a channel power threshold beyond which the Q-factor decreases much faster with the channel power due to the limited resolution of the reflection spectra. Therefore, the computational error in the results shown in Fig. 7, before the Q-factor decreased rapidly with the channel power, is the result of the Born approximation, which produces a computational error that increases as the channel power increases. Hence, the Born approximation can limit the use of the INFT algorithms for nonlinear mitigation. The reason why the performance of the system with 8 samples per symbol is worse than that with 2 samples per symbol at channel powers larger than −3.5 dBm is because the former system has only one quarter of the reflection spectra resolution of the latter, since the total number of points used to discretize the reflection spectra in these systems is fixed at 2^{15}.

Using the DLP algorithm in [30], the magnitude of the lumped local reflectance in (6) at the end of a time step Δt is given by

$$|\rho| = \tanh\left[\sqrt{\frac{\gamma}{|\beta_2|}}|A(t,z)|\Delta_t\right]. \tag{20}$$

The numerical approximation due to the lumping of the distributed reflection at the end of each step Δ_t requires that $|\rho| \ll 1$ for all layers. Since the normalization coefficient of the ZSSP in (3) for the optical fiber that we are considering is given by

$$\sqrt{\frac{\gamma}{|\beta_2|}} = 5.04 \times 10^{11}\ \mathrm{W}^{-1/2} \cdot s^{-1}, \tag{21}$$

we find that the average launch power per time step has to be below −3 dBm at 224 Gsamp/s per data frame for $|\rho| < 5\%$ at the center of a symbol. This rate corresponds, for example, to 56 Gbd per data frame with 4 samples per symbol. For 128 QPSK symbols per data frame with relative guard time $t_{g,R} = 1.2$, this limit corresponds to −5.8 dBm of channel power. As the magnitude of the local reflection increases, the approximation due to the lumping the reflection at the end of the layer becomes less accurate, leading to an increase in the computational error of the calculation of the waveform in each layer with duration Δ_t. This error accumulates during the layer peeling procedure. The magnitude of the lumped local reflection per layer close to the center of the symbols calculated for the results shown in Fig. 7 at −12 dBm of channel power are 5%, 2.5%, and 1.2% for 2, 4, and 8 points per symbol, respectively. These values of the lumped local reflection per layer (time step Δ_t) are much smaller than 1, as required by lumping the reflection at the end of the layer. However, at 0 dB of channel power, the corresponding magnitude of the local reflection is 19.7%, 9.9%, and 4.9% for 2, 4, and 8 samples per symbol, respectively. Therefore, the computational error that results from lumping the reflection at the end of the layer increases as the average launch power per data frame increases, which requires an increase in the number of samples per symbol used in the DLP algorithm. If the channel power is increased to 3 dBm, it would be necessary to have at least 16 samples per symbol to achieve $|\rho| < 5\%$. Even though the Fourier bandwidth of the waveform increases very little due to the nonlinear effects in the quasi-linear regimes that we investigated, an increase in the channel power requires an increase in the number of samples per symbol that is needed to minimize the error in the DLP method or in any other layer peeling method that relies on numerical approximations such as the Born approximation in the SILP. The increase in the number of samples used in the INFT algorithm can, in principle, be accomplished by interpolating the sampled values from the waveform.

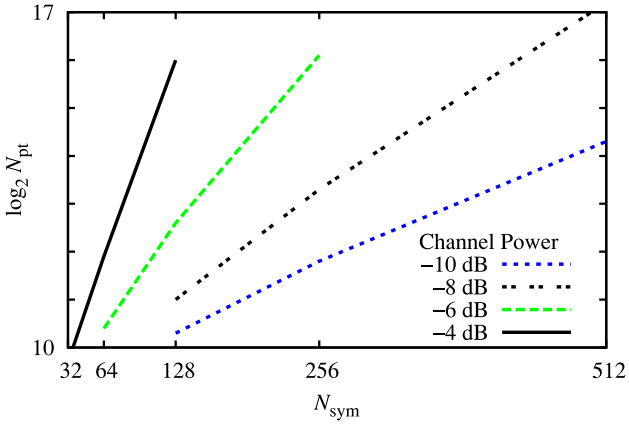

Fig. 8. The logarithm with base 2 of the number of points used to discretize each of the reflection spectra as a function the number of symbols per data frame (in linear scale) for $Q > 15$ dB due to the numerical error of the NFT-INFT algorithms. The symbol rate per data frame is equal to 56 GBd and the relative guard time $t_{g,R} = 1.2$. The results are parametrized by the channel power. The Q-factor is calculated from the EVM using 30 random data frames. The difference in dB between the channel power and the average launch power per data frame is given in Table I.

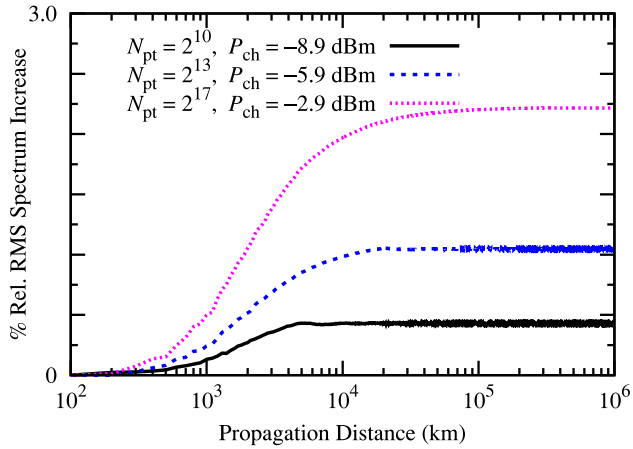

Fig. 9. The evolution along the fiber of the relative RMS width of the Fourier spectrum of the waveform that consists of 128 QPSK symbols with 56 GBd of symbol rate per data frame with relative guard time $t_{g,R} = 1.2$ for -8.8 dBm, -5.8 dBm, and -2.8 dBm of channel power with of channel power with 2^{11}, 2^{13}, and 2^{17} points to discretize both the reflection spectra and the time window of simulation, respectively. The results are calculated from the average of 30 random data frames. The channel power is -2.8 dB lower than the average launch power per data frame.

The Born (zero-order) approximation that is used in the numerical discretization of the SILP is given in terms of the kernel functions and the Fourier transform of the reflection spectra, as opposed to lumping the reflection at the end of each step Δ_t. However, accuracy in the SILP method also requires that $|\rho| \ll 1$. The computational error in the SILP accumulates slower than in the DLP during the iterative layer peeling procedure because of the higher numerical robustness of the SILP method.

D. NFT and Number of Symbols Per Data Frame

In Fig. 5, we observed the performance of the computational NFT in a QPSK modulation format at 56 GBd per data frame with 128 symbols per data frame and a minimum allowed value of $Q = 15$ dB due to numerical error. The maximum power was limited to -4 dBm using $N_{pt} = 2^{17}$ to discretize each of the reflection spectra. For a minimum allowed $Q = 15$ dB and 2^{17} points to discretize each of the reflection spectra for 256 and 512 symbols per data frame we observed that the channel power decrease to -6 dBm and -8 dBm, respectively. In Fig. 8 we show that the computational cost of the NFT-INFT algorithms increases exponentially with the number of symbols for a fixed channel power.

IV. Reflection Spectra Resolution

The numerical results shown in the previous section indicate that the eigenvalue resolution of the reflection spectra and, consequently, the computational cost of the NFT-INFT algorithms increases rapidly as the system moves from the linear to the quasi-linear regime of operation. The nonlinear effects in the optical fiber transmission system without in-line dispersion compensation, which requires the use of a fixed frame followed by a guard time, increase as a result of the increase in the channel power, in the number of symbols per data frame, or both. Since the practical viability of using computational NFT-INFT algorithms for nonlinear compensation in optical fiber communications systems depends significantly on the computational cost of the method, it is important to understand the reason for the interdependence between the computational cost of the NFT-INFT algorithms and both the channel power and the number of symbols per data frame. In what follows, we give an intuitive explanation for the rapid growth in computational cost with both the channel power and the data frame length for the NFT-INFT algorithm that we studied.

A. Reflection Spectra and Computation Time Window

Since the NFT based on the ZSSP described in Section II has a fixed value of the nonlinear parameter γ and the second-order dispersion β_2, there is always a finite propagation distance at which the non-zero region of the waveform centered at $T_w/2$ would disperse beyond the limits of the computation time window: $[0, T_w]$. Since T_w is in practical cases far larger than the signal frame, this distance will typically be larger than the propagation distance of 1,000 km. However, this distance always exists in the normal dispersion regime ($\beta_2 > 0$), since this regime does not support solitons. Once the waveform exceeds the upper or the lower limit of the simulation time window due to the chromatic dispersion, the signal appears at the opposite end of the simulation window in our computational algorithm due to the intrinsic periodicity that arises from our computational representation of the waveform. In our case, the eigenvalue resolution is given by $\Delta_\zeta = \pi/(N_{pt}\Delta_t)$ and $T_w = N_{pt}\Delta_t$. If the signal is still propagating nonlinearly when the periodic wrapping occurs, then the computational window is not large enough to resolve the nonlinear evolution. In this case, the INFT algorithm must produce a large error at any distance since its accuracy is the same at all distances.

In Fig. 9, we show the relative root-mean-square (RMS) width increase of the Fourier spectrum of a QPSK waveform with 128 symbols at 56 GBd per data frame with relative guard time $t_{g,R} = 1.2$ as a function of the propagation distance. The initial RMS width of the spectrum waveform at the origin is equal to 32.5 GHz. The RMS width of the Fourier spectrum increases until the dispersed waveform spreads out so much that the nonlinear effects become negligible or the dispersed waveform exceeds the simulation window. The total duration of the dispersed data frame T_{df} in the quasi-linear regime as a function of the propagation distance L is given by:

$$T_{\mathrm{df}} = N_{\mathrm{sym}} \cdot \frac{1}{f_{s,\mathrm{df}}} + 2\pi |\beta_2| f_{s,\mathrm{df}} \cdot L. \tag{22}$$

For the simulation with 2^{11} (for -8.8 dBm of channel power), 2^{13} (for -5.8 dBm of channel power), and 2^{17} (for -2.8 dBm of channel power) to discretize both the reflection spectra and the time window of simulation, the size of the periodic window is: 3.90×10^3 km, 15.5×10^3 km, and 331×10^3 km, respectively. These are the number of points used to discretize each of the reflection spectra that are the minimum to enable $Q > 15$ dB due to numerical error in the NFT-INFT algorithms. The number of points required to discretize the time window in most of the systems in the quasi-linear regime that we investigated is much larger than the number of points required to discretize each of the reflection spectra, since the actual propagation distance that we are considering, $L = 1,000$ km, is short compared to the propagation length in which the nonlinear effect is significant, as illustrated in Fig. 9. In the practical cases in which the number of samples recovered in time domain, N_{samp}, is smaller than the number of points used to discretize each of the reflection spectra, N_{pt}, the time shift in (14) has to be used.

B. Equivalence to Fiber Bragg Gratings

The left reflection spectra associated to the eigenvalues ζ in the ZSSP in (2) that models lossless transmission in optical fiber systems with normal dispersion is equivalent to the reflectance spectrum of a fiber Bragg grating, which can also be described by (2) [19]. The slowly varying envelope of a data frame in a normal dispersion fiber corresponds to the refractive index profile of an appropriate fiber Bragg grating:

1) A fiber Bragg grating with large value of the refractive index. This grating corresponds to a waveform with large optical power that is launched in an optical fiber with normal dispersion.
2) A wide fiber Bragg grating. This grating corresponds to a waveform with a long duration that is launched in an optical fiber with normal dispersion.

In both of these cases, the larger the refractive index of the fiber grating and/or the larger the fiber grating length, the closer to the maximum value of 1 the reflectance of the fiber grating will be over a wide spectral range. Likewise, in both of these cases, the narrower will be the frequency bands whose reflectance is significantly lower than 1, since constructive interference in the forward direction would take place in narrow bands that decrease with both the refractive index of the fiber grating and the fiber grating width. Therefore, the reflection spectra of the waveform launched in the corresponding optical fiber would also be close to 1 over a wide range of the eigenvalue ζ and the reflection spectra will be different from 1 in narrow eigenvalue bands whose widths decrease with the launch power and waveform duration at the transmitter. As a consequence, higher launch powers and a larger number of symbols per data frame require higher resolution of the reflection spectra.

The numerical error due to the Born approximation also increases with the the average launch power power, since the error per time step increases. Moreover, a larger number of symbols in the frame implies that more iterations are needed in the INFT algorithms, and the errors will accumulate due to the Born approximation. The combination of the finite reflection spectra resolution in the NFT algorithms and the Born approximation in the INFT algorithms that make use of that approximation leads to the exponential increase in the errors with both the channel power and the number of symbols per data frame that is shown in Figs. 5 and 8.

V. Conclusion

We used computationally efficient and robust computational methods to implement the NFT-INFT algorithms that work well when the reflection spectra are close to 1. We investigated the computational cost of nonlinear compensation techniques based on the NFT that is applied to optical transmission systems with normal dispersion fibers. We used the QPSK format with raised cosine spectral characteristic to show that the computational cost of the NFT-INFT algorithms increases exponentially or faster with both the channel power and with the number of symbols per data frame. We showed that the computational cost of the NFT is primarily limited by the eigenvalue resolution required for the reflection spectra in the NFT. If the INFT algorithm makes use of an iterative approximation along Δt, as does the SILP and other layer peeling methods, the number of samples per symbol must be large enough to satisfy that approximation. Since the computational NFT methods that we investigated require that the slowly varying envelope of the optical signal converges towards zero before the edges of the simulation window, the relative guard time has to be increased beyond $t_{g,R} = 1.2$ at higher power levels due to the increase in the spectral bandwidth along the propagation due to the fiber nonlinearity. This is a third, additional, effect that contributes to the decrease of the effectiveness of the NFT as a technique for nonlinear mitigation.

The NFT-INFT algorithm that we have studied is capable of reconstructing the waveform and its Fourier spectrum at any propagation distance. The distance over which the Fourier spectrum continues to increase can be orders of magnitude larger than the actual transmission distance when operating in the nonlinear regime, as shown in Fig. 9. The reflection spectrum must have sufficient resolution to resolve this entire evolution. If this condition is not satisfied, the computational error of the NFT-INFT algorithms will be large at any point along the transmission. For example, to use the NFT to process the signal that consists of 128 QPSK symbols at 56 GBd per data frame at -8.8 dBm of channel power, whose left reflection spectrum is shown in Fig. 2, the NFT requires only 2^{10} points to achieve $Q > 15$ dB. When the channel power is increased to -2.8 dBm,

the number of points required by the NFT to achieve $Q > 15$ dB for the same QPSK waveform increases to 2^{17}. For this system to operate at $Q > 15$ dB at 3 dBm, we estimate that the reflection spectra have to be discretized with at least 2^{103} points to process each QPSK frame with 512 symbols. The associated computational cost is not practical with currently available technology.

This study only explores data modulation in the time domain using the QPSK raised cosine modulation format. Le, *et al.* [10], carried out a study in which the signal was modulated directly in the left reflection spectrum in a transmission system that consisted of anomalous dispersion fibers. In that study, the peak performance was observed at only -4 dBm of average launch power per data frame, which was 3 dB above the peak performance of -7 dBm of average launch power per data frame produced by modulation in the time domain. Because of the guard time requirement due to the chromatic dispersion after 2,000 km of propagation distance, the actual channel power for peak performance in those two cases are -13.3 dBm and -16.6 dBm, respectively. We anticipate that extending this method to normal dispersion fibers is challenging. Systems with -2.8 dBm channel power, which corresponds to 0 dBm of average launch power per data frame with 128 symbols per data frame, in the normal dispersion regime have reflection spectra whose magnitudes are within 10^{-10} of 1 over a large portion of the reflection spectra. In the case that we considered, in which we directly modulated the slowly varying envelope of the optical signal, the maximum magnitude of the reflection spectra magnitude comes so close to 1 that it exceeds the accuracy of the floating point numerical representation at -1.2 dBm of channel power, which corresponds to 1.7 dBm of average launch power per data frame with 128 symbols per data frame, regardless of the number of points used to discretize each of the reflection spectra. While our results apply to a particular data format, we expect that the rapid increase of the required spectral resolution and, consequently, of the computational cost of the NFT algorithms with both the length of the data frame and the average launch power per data frame will hold generally. These issues should be addressed when assessing the practicality of the NFT with any modulation format.

REFERENCES

[1] P. J. Winzer and R.-J. Essiambre, "Advanced optical modulation formats," *Proc. IEEE*, vol. 94, no. 5, pp. 952–985, May 2006.

[2] A. Hasegawa and Y. Kodama, *Solitons in Optical Communications*. Oxford, U.K: Oxford Univ. Press, 1995.

[3] F. L. Mollenauer and J. P. Gordon, *Solitons in optical fibers - Fundamentals and Applications*. Amsterdan, The Netherlands: Elsevier, 2006.

[4] G. L. Lamb, *Elements of Soliton Theory*. New York, NY, USA: Wiley, 1980.

[5] M. J. Ablowitz and H. Segur, *Solitons and the Inverse Scattering Transform*. Philadelphia, PA, USA: SIAM, 1981.

[6] V. E. Zakharov and A. B. Shabat, "Exact theory of two-dimensional self-focusing and one-dimensional self-modulation of waves in nonlinear media," *Soviet Phys. JETP*, vol. 34, no. 1, pp. 62–69, 1972.

[7] M. I. Yousefi and F. R. Kschischang, "Information transmission using the nonlinear Fourier transform, Part I: Mathematical tools," *IEEE Trans. Inf. Theory*, vol. 60, no. 7, pp. 4312–4328, Jul. 2014.

[8] M. I. Yousefi and F. R. Kschischang, "Information transmission using the nonlinear Fourier transform, Part II: Numerical methods," *IEEE Trans. Inf. Theory*, vol. 60, no. 7, pp. 4329–4345, Jul. 2014.

[9] M. I. Yousefi and F. R. Kschischang, "Information transmission using the nonlinear Fourier transform, Part III: Spectrum modulation," *IEEE Trans. Info. Theory*, vol. 60, no. 7, pp. 4346–4369, Jul. 2014.

[10] S. T. Le, J. E. Prilepsky, and S. K. Turitsyn, "Nonlinear inverse synthesis for high spectral efficiency transmission in optical fibers," *Opt. Express*, vol. 22, no. 22, pp. 26 720–26 741, 2014.

[11] S. T. Le, J. E. Prilepsky, and S. K. Turitsyn, "Nonlinear inverse synthesis technique for optical links with lumbed amplification," *Opt. Express*, vol. 23, no. 7, pp. 8317–8325, 2015.

[12] S. Wahls, S. T. L. Jaroslaw, E. Prilepsky, H. V. Poor, and S. K. Turitsyn, "Digital backpropagation in the nonlinear Fourier domain," in *Proc. 2015 IEEE 16th Int. Workshop Signal Proc. Adv. Wireless Comm.*, 2015, pp. 445–447.

[13] M. I. Yousefi and X. Yangzhang, "Linear and nonlinear frequency division multiplexing," in *Proc. 42nd Eur. Conf. Opt. Commun.*, 2016, pp. 1–13.

[14] Z. Dong *et al.*,, "Nonlinear frequency division multiplexed based on NFT," *IEEE Photon. Tehcnol. Lett.*, vol. 27, no. 15, pp. 1621–1623, Aug. 2015.

[15] V. Aref, H. Bülow, K. Schuh, and W. Idler, "Experimental demonstration of nonlinear frequency division multiplexed Transmission," in *Proc. Eur. Conf. Opt. Commun.*, 2015, pp. 1–3.

[16] H. Bülow, V. Aref, and W. Idler, "Transmission of waveforms determined by 7 eigenvalues with PSK-modulated spectral amplitudes," in *Proc. Eur. Conf. Opt. Commun.*, 2016, pp. 412–414.

[17] V. Aref, S. T. Le, and H. Bülow, "Demonstration of fully nonlinear spectrum modulated system in the highly nonlinear optical transmission regime," in *Proc. 42nd Eur. Conf. Opt. Commun.*, 2016, pp 19–21.

[18] M. J. Ablowitz and J. F. Ladik, "Nonlinear differentia-difference equations and Fourier analysis," *J. Math. Phys.*, vol. 17, no. 6, pp. 1011–1018, 1976.

[19] G. Boffetta and A. R. Osborne, "Computation of the direct scattering transform for the nonlinear Schrödinger equation," *J. Comput. Phys.*, vol. 102, pp. 252–264, 1992.

[20] J. Skaar and O. H. Waagaard, "Design and characterization of finite-length fiber gratings," *IEEE J. Quantum Electron.*, vol. 39, no. 10, pp. 1238–1245, Oct. 2003.

[21] A. Rosenthal and M. Horowitz, "Inverse scattering algorithm for reconstructing strongly reflecting fiber Bragg gratings," *IEEE J. Quantum Electron.*, vol. 39, no. 8, pp. 1018–1026, Aug. 2003.

[22] S. Wahls and H. V. Poor, "Fast numerical nonlinear Fourier transforms," *IEEE Trans. Inf. Theory*, vol. 61, no. 12, pp. 6957–6974, Dec. 2015.

[23] S. Wahls and V. Vaibhav, "Fast inverse nonlinear Fourier transforms for continuous spectra of Zakharov-Shabat type," arXiv: 1607.01305v2, pp. 1–15, 2016. [Online]. Available: https://arxiv.org/abs/1607.01305

[24] J. Leuthold and W. Freude, *Optical OFDM and Nyquist multiplexing*, 6th ed. Amsterdan, The Netherlands: Elsevier, 2013, vol. VIB, ch. 9, pp. 381–432.

[25] E. G. Turitsina and S. K. Turitsyn, "Digital signal processing based on inverse scattering transform," *Opt. Lett.*, vol. 38, no. 20, pp. 4186–4188, 2013.

[26] I. T. Lima Jr., V. S. Grigoryan, M. O'Sullivan, and C. R. Menyuk, "Computational complexity of nonlinear transforms applied to optical communications systems with normal dispersion fibers," in *Proc. IEEE Photon. Conf.*, 2015, pp. 277–278.

[27] G. P. Agrawal, *Nonlinear Fiber Optics*, 3rd ed. San Diego, CA, USA: Academic, 2001.

[28] K. Chadan and P. C. Sabatier, *Inverse Problems in Quantum Scattering Theory*. New York, NY, USA: Springer, 1977.

[29] G. Song and S.-Y. Shin, "design of corrugated waveguide filter by the Gel'fand-Levitan-Marchenko inverse-scattering method," *J. Opt. Soc. Amer. A*, vol. 2, no. 11, pp. 1985–1915, 1985.

[30] R. Feced, M. N. Zervas, and M. A. Muriel, "An efficient inverse scattering algorithm for the design of nonuniform fiber Bragg gratings," *IEEE J. Quantum Electron.*, vol. 35, no. 8, pp. 1105–1115, Aug. 1999.

[31] A. Buryak, J. Bland-Hawthorn, and V. Steblina, "Comparison of inverse scattering algorithms for designing ultrabroadband fiber Bragg gratings," *Opt. Express*, vol. 17, no. 3, pp. 1995–2004, 2009.

[32] Y. Choi, J. Chun, and J. Bae, "Numerically extrapolated discrete layer-peeling algorithm for synthesis of nonuniform fiber Bragg gratings," *Opt. Express*, vol. 19, no. 9, pp. 8254–8266, 2011.

[33] O. V. Belai, L. L. Frumin, E. V. Podivilov, and D. A. Shapiro, "Efficient numerical method of fiber Bragg grating synthesis," *J. Opt. Soc. Amer. B*, vol. 24, no. 7, pp. 1451–1457, 2007.

[34] J. K. Proakis and M. Salehi, *Fundamentals of Communication Systems*, 2nd ed. Boston, MA, USA: Pearson, 2014.

[35] R. Schmogrow *et al.*,, "Error vector magnitude as a performance measure for advanced modulation formats," *IEEE Photon. Technol. Lett.*, vol. 24, no. 1, pp. 61–63, Jan. 2012.

[36] R. Schmogrow *et al.*, "Corrections to: Error vector magnitude as a performance measure for advanced modulation formats," *IEEE Photon. Technol. Lett.*, vol. 24, no. 23, p. 2198, Dec. 2012.
[37] O. V. Sinkin, R. Holzlöhner, J. Zweck, and C. R. Menyuk, "Optimization of the split-step Fourier method in modeling optical-fiber communications systems," *J. Lightw. Technol.*, vol. 21, no. 1, pp. 62–68, Jan. 2003.

Ivan T. Lima Jr. (SM'09) received the B.Sc. degree in electrical engineering (electronics) from the Federal University of Bahia, Salvador, Brazil, in 1995, the M.Sc. degree in electrical engineering (electromagnetics) from the University of Campinas, Campinas, Brazil, in 1998, and the Ph.D. degree in electrical engineering (Photonics) from the University of Maryland, Baltimore County, Baltimore, MD, USA, in 2003. He is a registered Professional Engineer in the State of North Dakota, USA. In 2003, he was an Assistant Professor in the Department of Electrical and Computer Engineering, North Dakota State University, Fargo, ND, USA. Since 2010, he has been an Associate Professor of Electrical and Computer Engineering with tenure at North Dakota State University. From October 2008 to August 2009, he was a Visiting Professor in the Department of Electrical and Computer Engineering, University of Manitoba, Winnipeg, MB, Canada. In Summer 2006, he was also a Faculty Fellow of the Air Force Research Laboratory at the Wright-Patterson Air Force Base in Dayton, Dayton, OH, USA. His research interests include biomedical engineering and optical fiber communications. He received the 2003 IEEE LEOS Graduate Student Fellowship Award and Venice Summer School on Polarization Mode Dispersion Award in 2003. He authored or coauthored 42 archival journal papers, 73 conference papers and presentations, two book chapters, one U.S. patent, and one provisional U.S. patent. He is a Senior Member of both the IEEE Photonics Society and The Optical Society (OSA). He is also a member of SPIE: The International Society for Optics and Photonics.

Thiago D. S. De Menezes received the B.S. degree in 2011 from the University of Campinas (UNICAMP), Brazil, and the Ph.D. degree in electrical and computer engineering in 2017 from North Dakota State University, Fargo, ND, USA. He received a Fulbright scholarship in 2009/2010 during his undergraduate studies for an exchange program with the U.S. Department of State. In 2011, he received a CAPES scholarship in partnership with UNICAMP and Michigan Technological University for a binational project on the social impact of digital divide in Brazil and in the United States. From 2015 to 2017, he collaborated with Ciena Corporation and the University of Maryland, Baltimore County, Baltimore, MD, USA, to investigate techniques for nonlinear mitigation in optical fiber communications systems. His research interests include fiber optical communications, digital signal processing, channel modeling, and simulation platform development.

Vladimir S. Grigoryan, biography not available at the time of publication.

Maurice O'Sullyvan, biography not available at the time of publication.

Curtis R. Menyuk (F'98) was born March 26, 1954. He received the B.S. and M.S. degrees from Massachusetts Institute of Technology, Cambridge, MA, USA, in 1976 and the Ph.D. degree from University of California of Los Angeles, Los Angeles, CA, USA, in 1981. He was a Research Associate at the University of Maryland, College Park, MD, USA and at Science Applications International Corporation in McLean, VA, USA. In 1986, he was an Associate Professor in the Department of Electrical Engineering, the University of Maryland Baltimore County, Baltimore, MD, USA, and he was the founding member of this department. In 1993, he was promoted to Professor. He was on partial leave from UMBC from Fall, 1996to Fall, 2002. From 1996 to 2001, he worked part-time in the Department of Defense, co-directing the Optical Networking program at the DoD Laboratory for Telecommunications Sciences in Adelphi, MD, USA, from 1999 to 2001. During 2001–2002, he was a Chief Scientist at PhotonEx Corporation. During 2008–2009, he was a JILA Visiting Fellow at the University of Colorado. For the last 30 years, his primary research interests include theoretical and computational studies of lasers, nonlinear optics, and fiber optic communications. He has authored or co-authored more than 280 archival journal publications as well as numerous other publications and presentations, and he is a co-inventor of five patents. He has also edited three books. The equations and algorithms that he and his research group at UMBC have developed to model optical fiber systems are used extensively in the telecommunications and photonics industry. He is a member of the Society for Industrial and Applied Mathematics and of SPIE. He is a Fellow of the American Physical Society, the Optical Society of America.. From 1996 to 1999, he was a Presidential Research Professo at UMBC, the winner of the 2013 IEEE Photonics Society William Streifer Award, and a 2015–2016 winner of the Humboldt Foundation Research Award.